Journal of Hydrology 529 (2015) 843–853

Contents lists available at ScienceDirect

Journal of Hydrology

journal homepage: www.elsevier.com/locate/jhydrol

Groundwater recharge assessment at local and episodic scale in a soil mantled perched karst aquifer in southern Italy

V. Allocca [a,*], P. De Vita [a], F. Manna [a], J.R. Nimmo [b]

[a] Dipartimento di Scienze della Terra dell'Ambiente e delle Risorse (DiSTAR), University of Naples Federico II, Via Mezzocannone, 8, Naples 80134, Italy
[b] U.S. Geological Survey, Menlo Park, CA, United States

ARTICLE INFO

Article history:
Received 1 June 2015
Received in revised form 4 August 2015
Accepted 17 August 2015
Available online 28 August 2015
This manuscript was handled by Peter K. Kitanidis, Editor-in-Chief, with the assistance of Barbara Mahler, Associate Editor

Keywords:
Groundwater recharge
Local and episodic scales
Perched karst aquifer
Soil cover
Water Table Fluctuation method

SUMMARY

Groundwater recharge assessment of karst aquifers, at various spatial and temporal scales, is a major scientific topic of current importance, since these aquifers play an essential role for both socio-economic development and fluvial ecosystems.

In this study, groundwater recharge was estimated at local and episodic scales in a representative perched karst aquifer in a region of southern Italy with a Mediterranean climate. The research utilized measurements of precipitation, air temperature, soil water content, and water-table depth, obtained in 2008 at the Acqua della Madonna test area (Terminio Mount karst aquifer, Campania region). At this location the aquifer is overlain by ash-fall pyroclastic soils. The Episodic Master Recession (EMR) method, an improved version of the Water Table Fluctuation (WTF) method, was applied to estimate the amount of recharge generated episodically by individual rainfall events. The method also quantifies the amount of precipitation generating each recharge episode, thus permitting calculation of the Recharge to the Precipitation Ratio (RPR) on a storm-by-storm basis.

Depending on the seasonally varying air temperature, evapotranspiration, and precipitation patterns, calculated values of RPR varied between 35% and 97% among the individual episodes. A multiple linear correlation of the RPR with both the average intensity of recharging rainfall events and the antecedent soil water content was calculated. Given the relatively easy measurability of precipitation and soil water content, such an empirical model would have great hydrogeological and practical utility. It would facilitate short-term forecasting of recharge in karst aquifers of the Mediterranean region and other aquifers with similar hydrogeological characteristics. By establishing relationships between the RPR and climate-dependent variables such as average storm intensity, it would facilitate prediction of climate-change effects on groundwater recharge. The EMR methodology could further be applied to other aquifers for evaluating the relationship of recharge to various hydrometeorological and hydrogeological processes.

1. Introduction

Karst aquifers represent about 12% of the Earth's continental area. About one quarter of the global population uses drinking water from these hydrogeological systems (Ford and Williams, 2007). Many European and Mediterranean countries are completely or partially dependent on groundwater resources of karst aquifers. In southern Italy, these aquifers are the main source for drinking water supplies (Celico, 1983; Celico et al., 2000; Allocca et al., 2007a, 2014) and they play also a vital role in groundwater-dependent fluvial ecosystems.

The mean annual yield of karst aquifers in southern Italy has been estimated to be about 4100×10^6 m^3 year^{-1}, with an average specific yield varying from 0.015 to 0.045 m^3 s^{-1} km^{-2} (Celico, 1983; Allocca et al., 2007a). This high productivity results from the high permeability of karst rocks, the occurrence of precipitation primarily during autumn and winter, and the presence of large summit endorheic or flat areas that favor infiltration and groundwater recharge processes (Manna et al., 2013a; Allocca et al., 2014). Another important feature of this region is the widespread existence of allochthonous soil mantles, comprising ash-fall pyroclastic deposits erupted by the main volcanic centers of the Campania region (De Vita et al., 2013). These surficial volcanic overburdens influence groundwater recharge, especially where they are relatively thick, by serving as temporary water storage that enhances evapotranspiration and modulates the percolation

* Corresponding author.
E-mail address: vincenzo.allocca@unina.it (V. Allocca).

http://dx.doi.org/10.1016/j.jhydrol.2015.08.032
0022-1694/© 2015 Elsevier B.V. All rights reserved.

of water into carbonate bedrock. At the same time, these deposits, in combination with abundant vegetation, limit the migration of microbial cells from the land surface to groundwater bodies (Naclerio et al., 2008, 2009; Bucci et al., 2015a, 2015b). The pyroclastic deposits also affect recharge processes by fostering the development of epikarst (Petrella et al., 2007; Celico et al., 2010).

Karst aquifers of southern Italy are characterized by a prevalent groundwater basal flow that emerges in major basal springs (Celico, 1978; Boni et al., 1986; Allocca et al., 2007b). By perched groundwater circulation, this basal flow feeds numerous high-altitude minor springs of importance for local water use.

To advance the techniques and understanding needed to assess groundwater recharge processes in different hydrogeological settings, and in particular to quantify and model the replenishment of groundwater by flow of infiltrated water through the unsaturated zone, is a fundamental and challenging issue (Lerner et al., 1990; Stephens, 1995; Scanlon et al., 2006; Healy, 2010). The importance of such advances is heightened by needs for sustainable management of groundwater resources, protection of fluvial ecosystems, assessing potential impacts of climate change on groundwater hydrology (VV.AA., 2007) (De Vita et al., 2012; Manna et al., 2013b; Hartmann et al., 2014a), and increasing demand for potable water (Wada et al., 2010). An important specific need is for hydrological studies on perched karst aquifers, as the related high-altitude spring outflows are a high-value water resource in mountainous areas.

Several direct and indirect methods have been developed for estimating groundwater recharge at regional to local spatial scales, and for annual to daily and episodic temporal scales (Andreo et al., 2008, 2014; Hartmann et al., 2014b; Fiorillo et al., 2014; Guardiola-Albert et al., 2014; Nimmo et al., 2015). One widely used technique is the Water Table Fluctuation (WTF) method (Healy and Cook, 2002). It has been infrequently applied to karst aquifers, perhaps because the water table is generally too deep for convenient monitoring. Various implementations of the WTF method have been developed, each having its own advantages and limitations (Todd, 1980; Coes et al., 2007). Examples include the RISE (Rutledge, 1998) and Master Recession Curve (MRC) methods (Heppner and Nimmo, 2005; Heppner et al., 2007; Lorenz and Delin, 2007; Delin et al., 2007), and other graphical approaches (Risser et al., 2005; Delin et al., 2007). Recently, Nimmo et al. (2015) developed an advancement of the WTF method, known as the Episodic Master Recession (EMR) method, to estimate episodic recharge at the local scales and to associate each recharge episode with a causal rainfall event. The EMR method has been tested (Nimmo et al., 2015) in a fractured sandstone aquifer (Masser Site, Pennsylvania, USA) and a glacial moraine aquifer (Silstrup Site, Denmark), but so far not in karst aquifers.

Our research proceeded through steps: (i) to estimate the recharge generated in individual storm-generated episodes in a one-year data record for a perched karst aquifer, along with the rainfall associated with each episode, to calculate the RPR; (ii) to quantitatively relate RPR values to the intensity of recharge-generating rainfall and to antecedent soil water content; and (iii) to test the computed average of RPR values against an independent estimate based on actual evapotranspiration evaluated using a soil water budget.

2. Description of the research site

The Acqua della Madonna test area is part of the central-southern sector of the Terminio Mount karst aquifer (Campania region, southern Italy), whose total extent is about 167 km^2 (Fig. 1a and b). The test area, of about 0.9 km^2 extent, is located at an altitude of about 1200 m a.s.l. (Fig. 1b and d) and is characterized by a perched karst aquifer that is constituted mainly by a fractured and partially karstified Cretaceous limestone series. The area is covered by alkali-potassic ash-fall pyroclastic deposits derived mainly from the Somma–Vesuvius volcano (Allocca et al., 2008). Over such pyroclastic deposits, Molli-Eutrisilic Andosols and Molli-Vitric Andosols are present, with thicknesses up to 0.50–0.60 m. In small karst plains (Fig. 1b) characterized by a mean slope angle lower than 3°, relatively deep bedrock, and pyroclastic mantle thickness up to 10–20 m, Pachi-Eutrisilic Andosols are developed (Allocca et al., 2008). Along hillslopes, deciduous forest (*Fagus sylvatica* L.) is the predominant land use type, whereas in the flat karst endorheic areas, grassland prevails (Allocca et al., 2008).

The limestone aquifer has very low primary porosity (about 0.1–0.6%) and a greater secondary porosity (about 2%), which is caused by a high degree of jointing and subordinately by the development of karst process along principal discontinuities. Several boreholes drilled to a depth of about 80 m in and near the test area (Fig. 1b and d), confirmed the existence of an unconfined karst aquifer under ash-fall pyroclastic deposits about 8 m thick. Due to the high altitude, with water-table levels ranging from 1151 to 1182 m a.s.l. (Fig. 1b and d), the Acqua della Madonna aquifer is perched with respect to the larger basal groundwater circulation, which feeds the main karst springs. Outflowing at altitudes from 330 to 473 m a.s.l at the base of the Mount Terminio aquifer, these springs vary from 0.1 to 1.4 m^3 s^{-1} in mean annual discharge. Boreholes in the test area have not revealed a stratigraphic or structural feature that would cause water to perch (Celico, 1988). Such features might be present below the depths reached by drilling, perhaps in low-permeability marls and clayey interbeds in the lower Cretaceous interval of the carbonate Mesozoic (D'Argenio et al., 1973), or in low-permeability Miocene inverse faults or thrusts that dislocate the carbonate series (Cello and Mazzoli, 1998).

The main boundaries determining lateral compartmentalization of the perched Acqua della Madonna aquifer (Fig. 1b) are Pleistocene direct fault systems that can act as barriers to flow, thus establishing a basin-in-series aquifer system (Petrella et al., 2009, 2014). In such a hydrogeological framework, high altitude springs are generally located in association with faults with a lower permeability of core zones (Fig. 1b and d). Limited groundwater flow, however, can occur through fault zones themselves, and may allow hydraulic exchanges among groundwater basins (Fig. 1d). The high altitudes of the springs and water table support the hypothesis of groundwater flow from northwest to southeast (Fig. 1b and d) through a well-connected fracture network. This flow feeds a seasonal spring (S1), with discharge up to 0.025 m^3 s^{-1} and two perennial springs (S2 and S3) with discharge from 0.005 m^3 s^{-1} to 0.15 m^3 s^{-1}. The water fluctuates through a range of several meters, and responds rapidly to substantial rainfall and related infiltration. During these fluctuations, the water table is sometimes within the pyroclastic soil mantle and sometimes within the fractured carbonate bedrock (Fig. 1c). Recharge of the perched karst aquifer mostly occurs from September to May. After major precipitation events, mostly between December and April, recharge is primarily autogenic, from net infiltration and percolation through the vadose zone.

The main physical and hydraulic properties of the perched karst aquifer (Table 1) were determined by field and laboratory tests (Allocca et al., 2008; Naclerio et al., 2009). Water-table levels were measured and monitored in the P1 borehole (60 m deep), through 8.5 m of pyroclastic deposits and 51.5 m of calcareous rock-mass (Fig. 1c).

The climate of the study area is a Mediterranean-mild (CSb) type (Geiger, 1954). Allocca et al. (2014) developed a hydrometorological characterization of the area on the basis of 90 years (1920–2012) of data from a regional meteorological network and extrapolation of these data to higher altitudes. The estimated mean

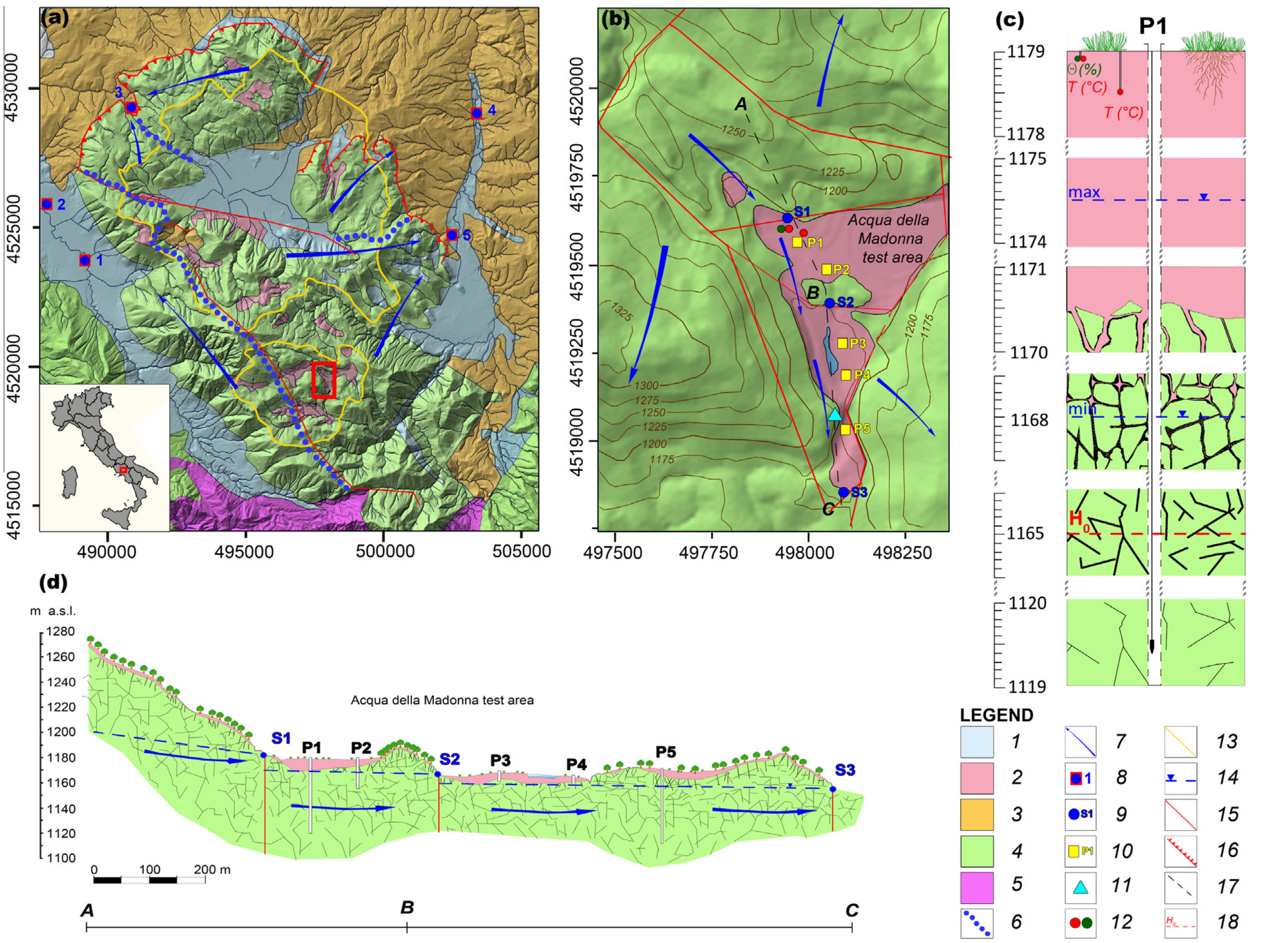

Fig. 1. (a) Hydrogeological map of Terminio Mount karst aquifer. (b) Hydrogeological map of Acqua della Madonna perched aquifer. (c) Hydrostratigraphic scheme of piezometer P1. (d) Hydrogeological section of Acqua della Madonna perched aquifer. Key to symbols: (1) Alluvial units (Quaternary); (2) Ash-fall units (Quaternary); (3) Terrigenous units (Cretaceous-Pliocene); (4) Limestone unit (Cretaceous); (5) Dolomitic unit (Trias); (6) Hydrogeological divide; (7) Main groundwater flow direction; (8) Basal springs [(1) Acquaro-Pelosi spring, 376 m a.s.l.; (2) Urciuoli spring, 330 m a.s.l.; (3) Sauceto spring, 465 m a.s.l.; (4) Baiardo spring, 470 m a.s.l.; (5) Cassano Irpino spring, 473 m a.s.l.]; (9) Perched springs [(S1) Verteglia spring 1182 m a.s.l.; (S2) Acqua della Madonna spring, 1168 m a.s.l.; (S3) Giumenta spring, 1151 m a.s.l.]; (10) Piezometers; (11) Meteorological station; (12) Soil temperature (red circle) and soil–water content (green circle) sensors; (13) Morphological divide of endorheic basin; (14) Water table level (min and max); (15) Faults; (16) Thrusts; (17) Cross section trace; (18) Reference datum for water table level. (For interpretation of the references to color in this figure legend, the reader is referred to the web version of this article.)

annual rainfall for the Mount Terminio karst aquifer is 1730 mm, the mean annual air temperature is 8.4 °C. The estimated average annual groundwater recharge is 1280 mm, about 74% of the mean annual precipitation.

3. Data and methodologies

3.1. Hydrological monitoring

For use in evaluating groundwater recharge episodes at the local scale, daily thermo-pluviometric time series recorded by meteorological stations of the Regional Civil Protection Agency were collected from January to December 2008 (Fig. 2a). For the same period, hourly groundwater levels were measured in the piezometer P1 by a pressure transducer (STS Inc., USA) and datalogger (Figs. 1b, c and 2a). In addition, volumetric soil water content ($\theta = V_w/V_t$) data were measured hourly by a transducer with datalogger (SIAP-MICROS Inc., Italy) at a depth of 0.10 m (Figs. 1b, c and 2c). This depth was chosen as representative of the upper unsaturated zone, which is exposed to evapotranspiration processes dominated by the roots of grassy vegetation to about 0.6 m deep.

3.2. Estimation of groundwater recharge at episodic and local scale

To assess local-scale groundwater recharge of the Acqua della Madonna aquifer generated during individual episodes, we adopted the Episodic Master Recession (EMR) method (Nimmo

Table 1
Physical and hydraulic properties of the perched karst aquifer (Allocca et al., 2008; Bucci et al., 2015a, 2015b; Naclerio et al., 2009).

Aquifer layer	Soil texture type (%)			Saturated thickness (m)		Specific yield (%)	Hydraulic conductivity (m/s)
	Gravel	Sand	Silt	Min	Max		
Pyroclastic deposits	5	86	9	0	4	5	5.6×10^{-5}
Fractured carbonate bedrock				>49	>51.5	2	4.7×10^{-7}

et al., 2015), which is an extension of the Water Table Fluctuation (WTF) approach (Meinzer, 1923; Healy and Cook, 2002). This method uses the measured water-table height (H), with respect to a datum corresponding to the position of the water table in the absence of episodic recharge. It estimates recharge during an episode as

$$R_j = S_y \times \Delta H_j, \tag{1}$$

where R_j (mm) is the amount of groundwater recharge during the jth episode; S_y (%) is the specific yield; and ΔH_j (mm) is the extent of water table rise during the jth episode. The determination of ΔH_j is complicated by groundwater recession and other processes going on during the period of water-table rise. In the EMR method ΔH_j is computed using extrapolations of the time-series $H(t)$ from intervals of recession before and after the recharge episode.

The first step in applying this method is to develop an optimized MRC, the characteristic rate of water-table decline as a function of H, for the given well or location. This curve is determined using a subset of the $H(t)$ data selected as representing pure water-table recession. After numerically computing dH/dt from these data and by regression determining an optimized dH/dt as a function of H, the EMR algorithm uses this MRC to delineate the recharge episodes. An episode is recognized when the observed water-table rate of change (dH/dt) exceeds that predicted by the MRC (dH/dt_{MRC}), by an amount greater than a previously established fluctuation tolerance (Fig. 3a). The time when this exceeding of the tolerance band occurs is called the breakout time. The start of a single recharge episode is taken as the time at which the observed dH/dt crosses the computed dH/dt_{MRC} curve (the center of the tolerance band) before the breakout time. The start time, however, is constrained to not precede the breakout time by more than the lag time of the system, previously identified as the time required for newly infiltrated water to arrive at the water table. Similarly, the end of the recharge episode is taken as the time when dH/dt crosses the computed dH/dt_{MRC} from below, after it reenters the tolerance band (Fig. 3a). The recharge in a single episode is the product of the specific yield and the difference, taken at the time of the water-table peak, of two H values extrapolated from the recession limbs that precede and follow the recharge episode (Fig. 3b). Thus for each recharge episode, the EMR algorithm calculates start (t_o) and end (t_f) times (Fig. 3a and b), which indicate episode duration (D), and groundwater recharge (G_R).

The precipitation event associated with a recharge episode begins one lag time before the start, and ends one lag time before the end of the recharge episode (Fig. 3a). The Recharge to Precipitation Ratio (RPR) for each recharge episode is calculated by

$$\mathrm{RPR}_j = \frac{G_{Rj}}{P_j}, \tag{2}$$

where G_{Rj} (mm) is the groundwater recharge for the jth recharge episode and P (mm) is the precipitation for the jth recharge episode.

To apply the EMR technique, water-table levels measured from January to December 2008 were referred to a datum (H_0) lying at 1165 m a.s.l. (Fig. 1c). The aquifer response time was calculated by a cross-correlation analysis between precipitation and water-table level (Fig. 2a and b); the same approach was used to find the correlation between precipitation and θ (Fig. 2c and d). Finally, to assess the influence on episodic groundwater recharge of other basic hydrological factors that control processes of infiltration and percolation to the water table, a multiple regression analysis was performed between the RPR values and the average intensity of the recharging rainfall events and antecedent soil–water content. The antecedent soil–water content was defined as the average soil–water content (θ_{av}), measured at a depth of 0.10 m three days before the onset of rainfall.

3.3. Soil water balance

To further understand vadose zone hydrological processes, we estimated potential evapotranspiration using available hydrological data at the monthly time-scale by Thornthwaite (1948) method:

$$\mathrm{Ep}_i = K \times \left[1.6 \times \left(\frac{t_i}{I}\right)^{\alpha}\right], \tag{3}$$

where Ep_i (mm) is the mean potential evapotranspiration for the ith month; K is a dimensionless coefficient that depends on the mean monthly duration of solar radiation for the month of the year and

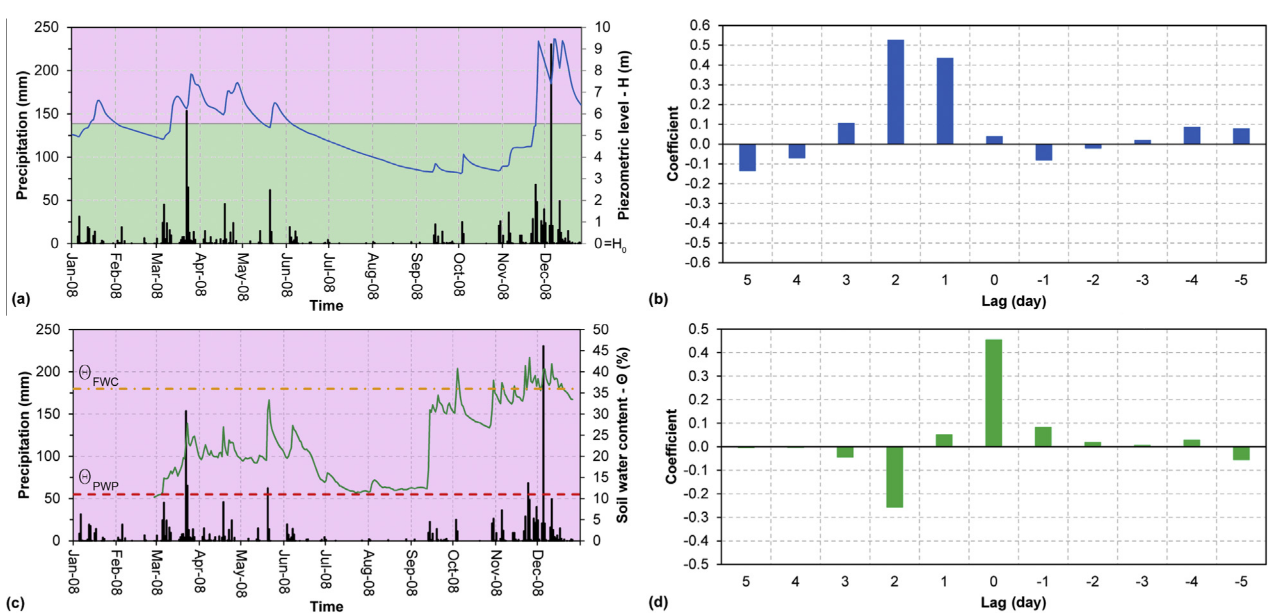

Fig. 2. (a) Time series of piezometric level (blue line) and precipitation (black histogram). The background color represents the interval of depths for fractured carbonate substrate (green) and pyroclastic deposits (pink). (b) Cross-correlation analysis between piezometric level and precipitation. (c) Time series of soil–water content at 10 cm depth (green line) and precipitation (black histogram). (d) Cross-correlation analysis between soil–water content at 10 cm depth and precipitation. (For interpretation of the references to color in this figure legend, the reader is referred to the web version of this article.)

latitude; t_i is the mean air temperature for the ith month (°C); I is the annual heat index (dimensionless); α is an exponent given by

$$\alpha = 675 \times 10^{-9} \times I^3 - 771 \times 10^{-7} \times I^2 + 1792 \times 10^{-5} \times I + 0.49239. \tag{4}$$

The monthly actual evapotranspiration (ETR_i) was calculated by the soil water balance method (Thornthwaite and Mather, 1955, 1957). Besides Ep_i, this method considers the monthly precipitation (P_i) and the total available water content ($\Delta\theta_{TAW}$) in the evapotranspiration zone, corresponding to the difference between a field capacity value (θ_{FWC}) and Permanent Wilting Point (θ_{PWP}). During the humid season, water content in the evapotranspiration zone typically reaches the θ_{FWC} value, so that the stored amount of soil moisture available for the evapotranspiration is at its maximum ($\Delta\theta_{TAW}$) and ETR_i is equal to Ep_i. If the soil–water content exceeds the θ_{FWC} under these conditions due to rainfall, runoff (R_i) and net infiltration (I_{ei}) increase, and groundwater recharge occurs. Conversely, during months when rainfall is less than Ep_i, ETR_i can equal Ep_i due to the loss of water stored in the evapotranspiration zone in the preceding month ($\theta_{i-1} - \theta_{PWP}$). Therefore, in the humid season, defined as the time interval when

$$P_i + (\theta_{i-1} - \theta_{PWP}) - Ep_i \geqslant 0, \tag{5}$$

monthly groundwater recharge, or monthly effective net infiltration (I_{ei}), is given by:

$$I_{ei} = [P_i + (\theta_{i-1} - \theta_{PWP}) - Ep_i] - R_i. \tag{6}$$

Finally, when no soil moisture for the evapotranspiration zone is available ($\theta = \theta_{PWP}$), ETR_i is lower than Ep_i ($ETR_i < Ep_i$) and corresponds to monthly rainfall (P_i). Consequently in the dry season, defined by

$$P_i + (\theta_{i-1} - \theta_{PWP}) - Ep_i \leqslant 0, \tag{7}$$

no groundwater recharge episodes or runoff occur.

Owing to the flat and endorheic geomorphological features of the Acqua della Madonna test area, which permits negligible runoff toward the altimetrically lowest sector, monthly and annual amounts of water surplus estimated by the soil water balance method, were considered, as an approximation, to contribute to groundwater recharge only.

θ_{FWC} and θ_{PWP} were respectively set equal to 36.9% and 11.0%, based on retention curves measured on undisturbed pyroclastic soil samples (De Vita et al., 2013). Therefore the $\Delta\theta_{TAW}$ value was equal to 26.0%. Knowing the maximum rooting depth (Fig. 1c) of local vegetation to equal 0.60 m (Bucci et al., 2015a; Keller and Bliesner, 1990), the estimated equivalent water height $\Delta\theta TAW$ is 156 mm.

4. Results

4.1. Aquifer response time

During 2008, water-table levels observed in the piezometer P1 and measured with respect to the considered datum

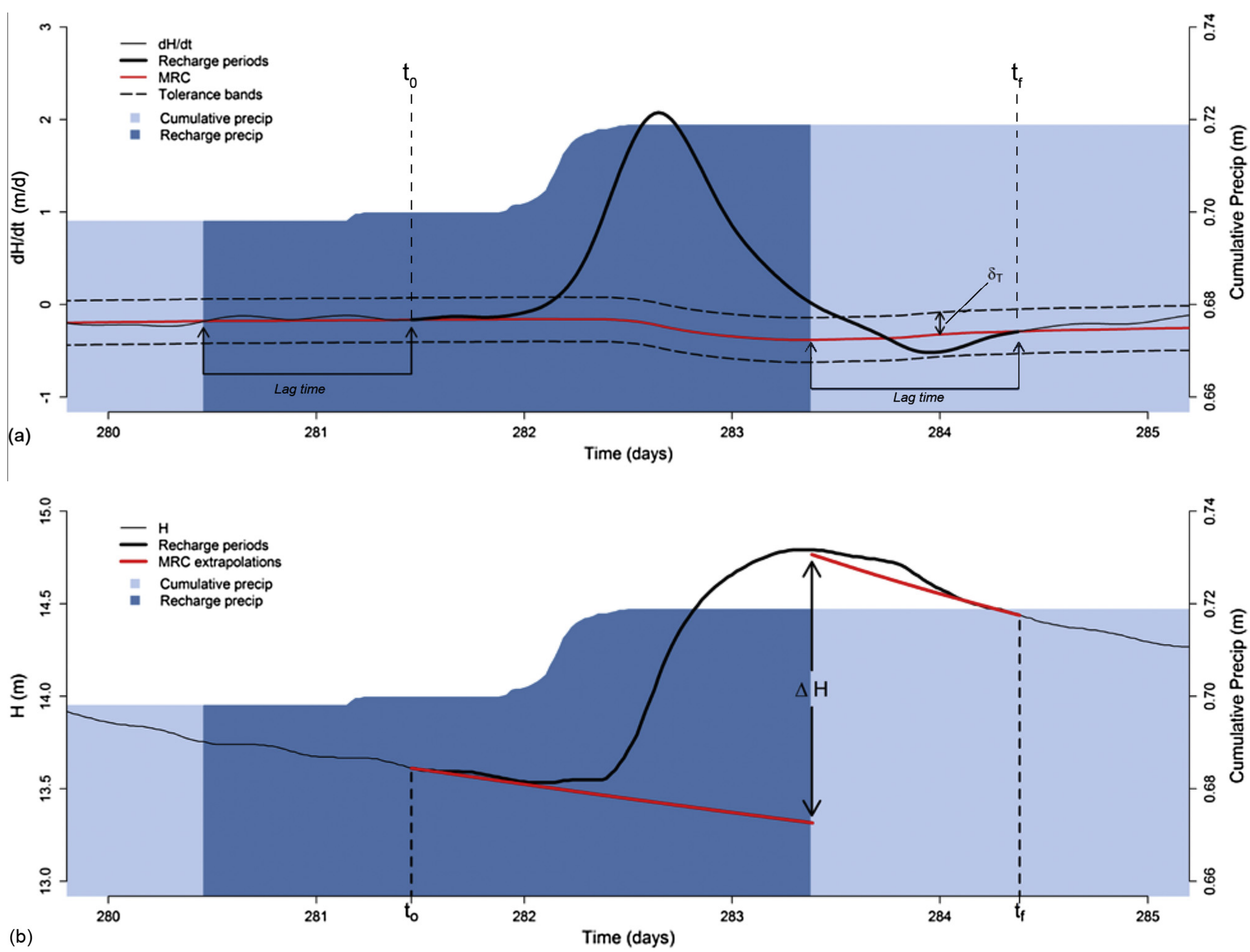

Fig. 3. EMR method. (a) Detection of the recharge episodes based on dH/dt analysis. (b) Determination of the ΔH between the two MRC extrapolations. Adapted from Fig. 3 of Nimmo et al. (2015).

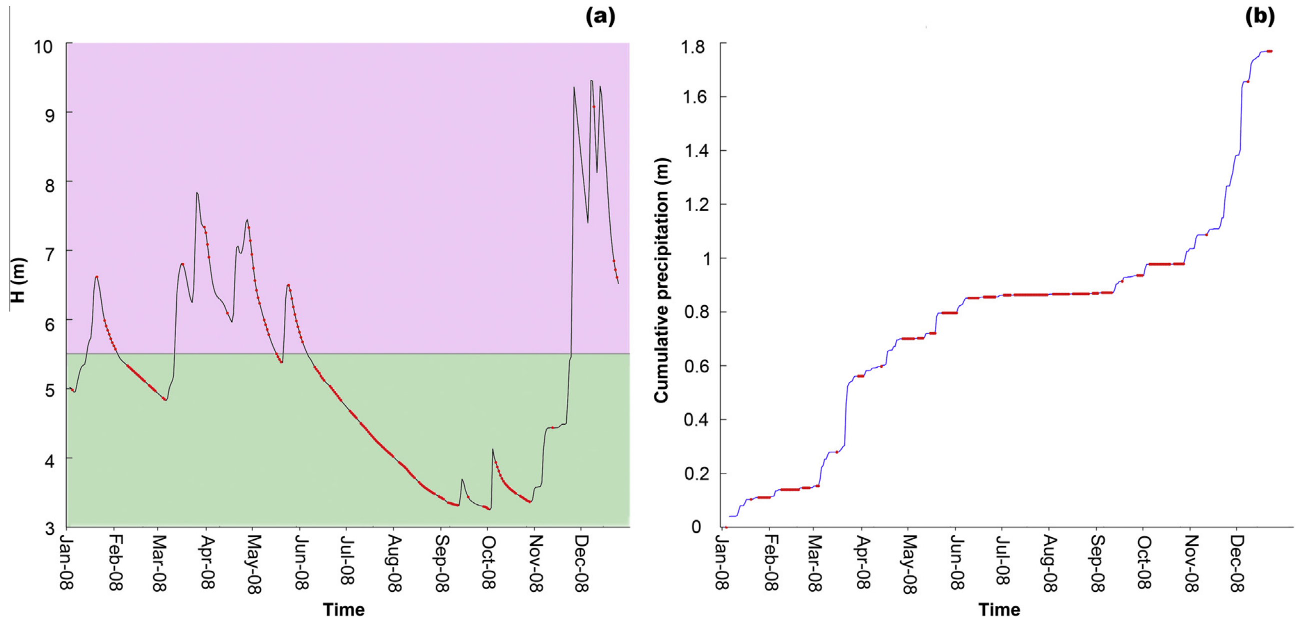

Fig. 4. (a) Time series of piezometric level (H level referred to H_0 = 1165 m a.s.l.) with pure recessional data (red points). (b) Cumulative precipitation and pure recessional data (red points). The background colors represent the fractured carbonate substrate (green) and pyroclastic deposits (pink). (For interpretation of the references to color in this figure legend, the reader is referred to the web version of this article.)

(H_0 = 1165 m a.s.l.) varied between +3.2 m and +9.4 m, with an average of +5.2 m (Fig. 2a). The minimum level was recorded on the 2nd of October, at the end of a major recession period that coincided with the summer season of little rainfall (2.4 mm in July and 6.2 mm in August). The maximum value was detected at the beginning of December.

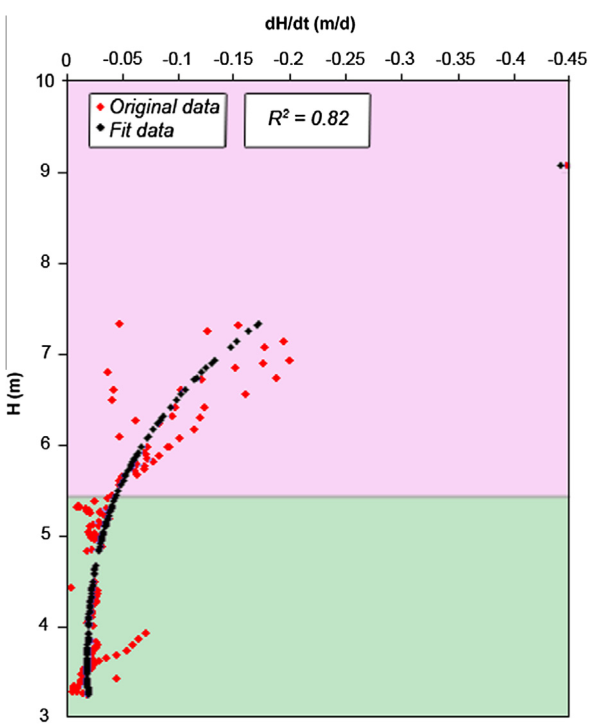

Fig. 5. Master Recession Curve (MRC) for P1 piezometer. Red points represent the pure recession data (Fig. 4); black points represent the Master Recession Curve. The background colors represent the fractured carbonate substrate (green) and pyroclastic deposits (pink). (For interpretation of the references to color in this figure legend, the reader is referred to the web version of this article.)

During the recession periods, water-table levels decreased gradually (Fig. 2a) and rose rapidly after rainfall, at rates up to 0.92 m day^{-1}. The correlation between rainfall and water-table time series was significant, indicating a clear and fast aquifer response. The maximum correlation was found at a time lag of 2 days (Fig. 2b) (r = 0.53; prob. t-Student < 0.1%), which was considered to equal the storm recovery time. In addition, the θ time series reflects the temporal pattern of daily precipitation (Fig. 2c), with highest value during the winter season (43.0%) and lowest during the summer (10.0%). The temporal analysis (Fig. 2c) shows three phases during which θ remains within a relatively narrow range: the first phase, March to June, had a mean value of 20.0%; a second phase, in summer, July to September, had a mean value of 12.0%; and a third phase, October to December, had the highest mean value of 35.0%. A significant cross-correlation between θ and rainfall time series was found (Fig. 2d) with a time lag of 0 (r = 0.450; prob. t-Student < 0.1%).

Recharge occurs also under soil–water conditions drier than the θ_{FWC} value (Fig. 2a and c). This observation, which counters conventional expectations for the soil water balance and groundwater recharge, could result from thin-channel preferential flow phenomena (Mirus and Nimmo, 2013) which are among the possible unsaturated zone processes under relatively dry conditions (Nimmo, 2012). Such a localized effective infiltration process can also explain the lack of observed concurrent increases in water content.

4.2. Episodic groundwater recharge

The water-table level time-series recorded by the piezometer P1 during 2008 was analyzed by an MRC algorithm that automatically identifies subsets corresponding to recessional limbs of $H(t)$ (Fig. 4). The MRC was constructed as an empirical correlation between dH/dt and H (Fig. 5), fitting recorded data with a third order polynomial (r = 0.906; prob. t-Student < 0.1%). Considering apparent changes in slope of the data trend, it would alternatively be possible to split the entire dataset into two parts, above and below the interface, at H = 5.4 m, between the pyroclastic soil

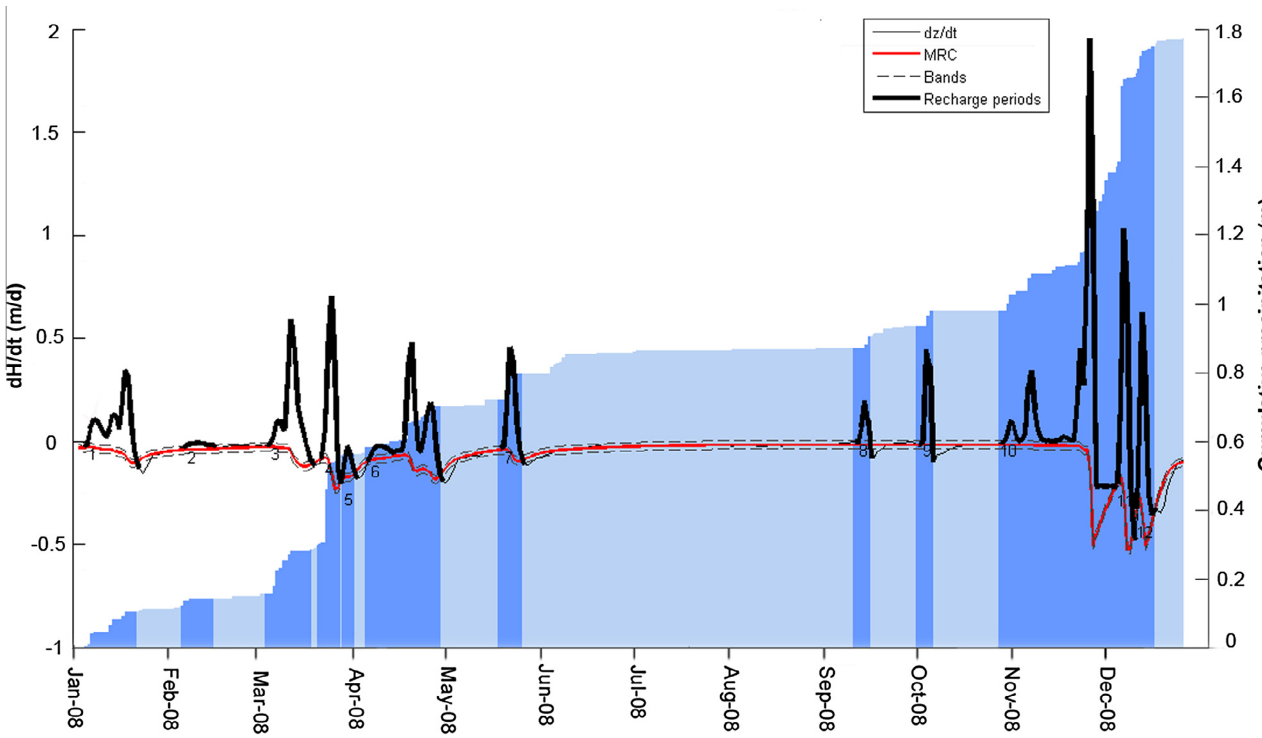

Fig. 6. Episodic Master Recession analysis of dH/dt versus time. The numbers identify the recharge episodes.

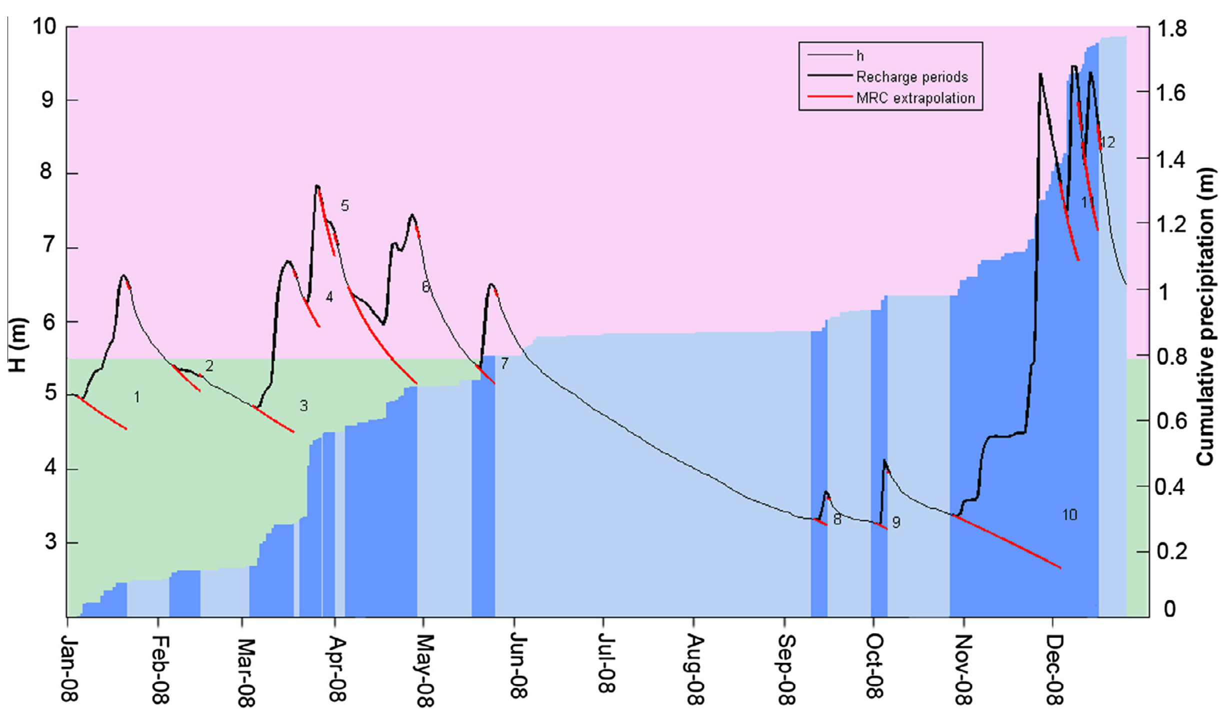

Fig. 7. Episodic Master Recession analysis of H versus time. The background colors represent the fractured carbonate substrate (green) and pyroclastic deposits (pink); the numbers identify the recharge episodes. (For interpretation of the references to color in this figure legend, the reader is referred to the web version of this article.)

and the karst medium. Each part would then have a distinctly different slope of dH/dt; decline rates vary from 0.00 to 0.05 m day^{-1} in the karst, and from 0.05 to 0.45 m day^{-1} in the pyroclastic soil (Fig. 5). This difference was related to a composite model with the two hydrostratigraphic layers having different geometry, saturated-zone thickness, specific yield, and hydraulic conductivity (Fig. 1c and d, and Table 1). Specifically, the pyroclastic material, besides a greater specific yield, has a thinner saturated zone and higher hydraulic conductivity than the underlying karst. These characteristics likely determine the greater dH/dt values in the pyroclastic interval.

The analysis of water-table levels time series recognized 12 recharge episodes (Figs. 6 and 7). Episode durations ranged from 5 to 37 days, with a mean value of 12 days, whereas the length

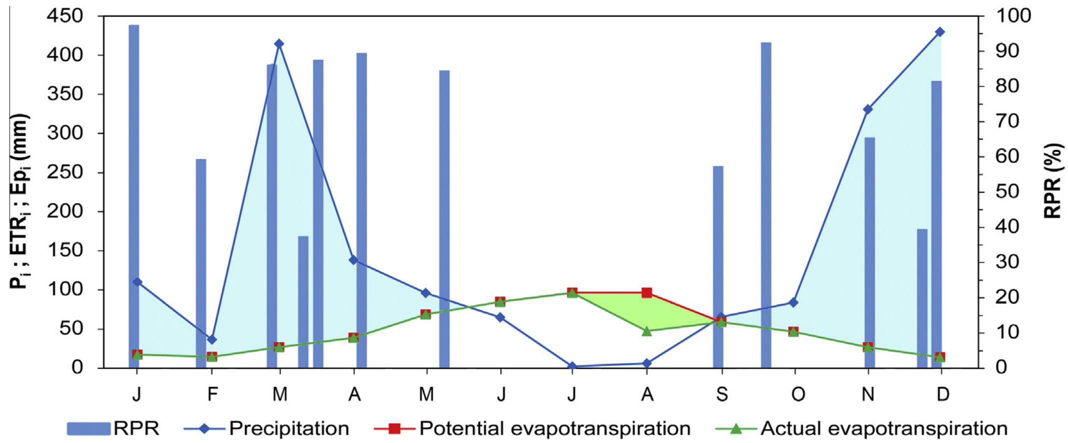

Fig. 8. Monthly soil water balance carried out for 2008 by the Thornthwaite and Mather method (1955, 1957). The blue histogram represents groundwater recharge episodes and related values of RPR values. Blue area refers to the soil water surplus and the green area refers to the soil water deficit. (For interpretation of the references to color in this figure legend, the reader is referred to the web version of this article.)

of non-recharge periods varied from 0 to 107 days, the longer ones occurring in summer. The first nine recharge episodes showed relatively low values of dH/dt, from 0.25 to 0.60 m day^{-1}, while episodes 10, 11, and 12 showed greater dH/dt, as high as about 2 m day^{-1} in episode 10.

Values of RPR, calculated using the EMR method and Eq. (2), range from 35% to 97%, with a mean annual value of 73% (Table 2 and Fig. 8). This result was compared to that of an independent method based on a monthly soil water balance for 2008 by the Thornthwaite and Mather (1955, 1957) method. Monthly actual evapotranspiration (ETR_i) was always maximal (equal to potential evapotranspiration Ep_i) during the months from January to July and from September to December; in these months there was a soil water surplus that allowed groundwater recharge (Fig. 8). In August, ETR_i was less than Ep_i, indicating a condition of soil water deficit (Fig. 8) with no apparent possibility of groundwater recharge.

Potential evapotranspiration (Ep) totaled about 591.6 mm for the year, corresponding to 33% of P, whereas actual evapotranspiration (ETR) amounted totally to 542.8 mm, corresponding to 30% of P. These estimates closely match the complement of the mean annual value of episodically calculated RPR (27%), demonstrating good agreement of the two approaches to recharge estimation.

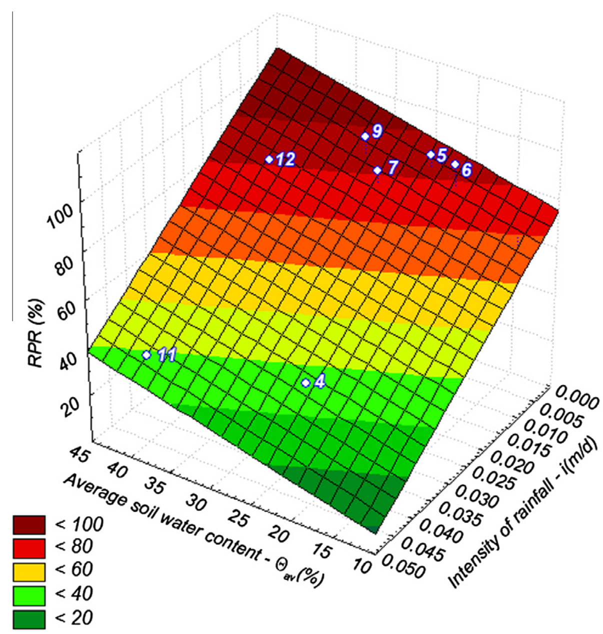

Fig. 9. Multiple linear regression between RPR, antecedent average soil–water content and average intensity of recharging rainfall events. The colors represent the RPR values and the numbers the recharge episodes.

Table 2
Characteristics of the recharge episodes.

Recharge episodes	Start time t_i (day)	End time t_f (day)	Duration D (day)	Groundwater recharge G_R (m)	Precipitation P (m)	Recharge to precipitation ratio RPR (%)	Av. storm intensity i (m/day)	Max storm intensity i_{max} (mm/day)	Average soil–water content (θ_{av}) (%)
1	04 Jan	21 Jan	18	0.1	0.104	97	0.006	31.4	–
2	05 Feb	15 Feb	10	0.011	0.019	59	0.002	19.2	–
3	03 Mar	18 Mar	15	0.11	0.129	86	0.009	45.2	–
4	21 Mar	27 Mar	6	0.093	0.247	37	0.038	153.6	23.49
5	28 Mar	01 Apr	5	0.014	0.017	87	0.003	4.6	24.16
6	05 Apr	29 Apr	24	0.107	0.12	89	0.005	46	20.45
7	18 May	26 May	8	0.064	0.076	84	0.01	62	27.78
8	10 Sep	16 Sep	5	0.019	0.033	57	0.006	22.4	12.42
9	01 Oct	06 Oct	5	0.039	0.042	92	0.008	25	30.51
10	27 Oct	03 Dec	37	0.261	0.404	65	0.011	68.4	34.01
11	05 Dec	10 Dec	6	0.107	0.272	39	0.046	230.6	39.45
12	12 Dec	17 Dec	6	0.072	0.089	81	0.014	49.2	39.42

Table 3
Results of the Thornthwaite and Mather water balance. Key to symbols: Ep_i' = unadjusted potential evapotranspiration for the ith month; Ep_i = adjusted potential evapotranspiration for the ith month; P_i = precipitation for the ith month; Δ_i = precipitation minus potential evapotranspiration for the ith month; A_i = soil storage for the ith month; ΔA_i = change in soil storage for the ith month; ETR_i = actual evapotranspiration for the ith month; S_i = water surplus for the ith month; D_i = water deficit for the ith month.

Parameters	Jan	Feb	Mar	Apr	May	Jun	Jul	Aug	Sep	Oct	Nov	Dec	Tot
Air T (°C)	5.9	5.0	7.4	9.8	15.4	18.9	21.2	22.7	15.9	13.6	9.2	4.9	
Heat index (I)	1.3	1.0	1.8	2.8	5.5	7.5	8.9	9.9	5.8	4.5	2.5	1.0	52.4
Ep_i' (mm)	20.9	17.7	26.3	35.1	55.1	67.5	75.8	81.0	56.9	48.6	32.9	17.6	535.4
Adjustment factor	0.8	0.8	1.0	1.1	1.3	1.3	1.3	1.2	1.0	1.0	0.8	0.8	
Ep_i (mm)	17.4	14.7	27.1	39	68.8	85.0	96.3	96.4	59.2	46.6	27.0	14.1	591.6
P_i (mm)	110.2	36.6	414.6	138.2	96.2	65.0	2.4	6.2	65.6	84.2	330.8	429.8	1779.8
Δ_i (mm)	92.8	21.9	387.5	99.2	27.4	−20.0	−93.9	−90.2	6.4	37.6	303.8	415.7	1188.2
A_i (mm)	155.4	155.4	155.4	155.4	155.4	135.4	41.4	0.0	6.4	44.0	155.4	155.4	1315.0
ΔA_i (mm)	0.0	0.0	0.0	0.0	0.0	−20.0	−93.9	−41.4	6.4	37.6	111.4	0.0	0.0
ETR_i (mm)	17.4	14.7	27.1	39.0	68.8	85.0	96.3	47.6	59.2	46.6	27.0	14.1	542.8
S_i (mm)	92.8	21.9	387.5	99.2	27.4	0.0	0.0	0.0	0.0	0.0	192.4	415.7	1237.0
D_i (mm)	0.0	0.0	0.0	0.0	0.0	0.0	0.0	48.8	0.0	0.0	0.0	0.0	48.8

4.3. Dependence of RPR on soil–water content and rainfall intensity

The comparison of groundwater recharge dynamics (Table 2) with rainfall patterns and seasonality allowed an assessment of possible trends in RPR values with respect to rainstorm intensity and antecedent soil–water content. For example, the two lowest RPR values of 37% and 39%, from episodes 4 and 11, corresponded to the highest rainfall intensities of 0.038 m day^{-1} and 0.046 m day^{-1}. Moreover, the observed groundwater recharge episodes (Figs. 7 and 8) suggest a direct relationship between antecedent soil–water content and RPR, lower water content leading to lower RPR. Recharge episode 8 (September 2008), for example, was characterized by a modest RPR of 57%, notwithstanding the low rainfall intensity of about 0.006 m day^{-1}. This observation suggests a possible influence during this period of the seasonal soil water deficit on episodic recharge. By multiple linear regression of RPR values, average rainfall intensities (i), and average soil–water content (θ_{av}) estimated for the 12 episodes (Table 2), we found a relation between the dependent variable RPR and the other two independent variables (Fig. 9; r = 0.894; prob. t-Student < 0.1%):

$$\text{RPR } (\%) = 0.67 + 0.8 \cdot \theta_{av} - 13.41 \cdot i. \tag{8}$$

This empirical equation is expected to apply in the ranges of the observed variables (Table 2): $37\% \leqslant \text{RPR} \leqslant 97\%$; $10.0\% \leqslant \theta_{av} \leqslant 43.0\%$; $0.001 \text{ m day}^{-1} \leqslant i \leqslant 0.046 \text{ m day}^{-1}$. Its form confirms the opposite-direction influences of both independent variables (θ_{av} and i) and the greater sensitivity of RPR to rainfall intensity than to average water content.

5. Discussion

This research is a first attempt to estimate groundwater recharge at the local and episodic scales in this area or similar areas. Related research has been carried out at the aquifer and mean annual scales for karst aquifers of southern Italy by estimating the Annual Groundwater Recharge Coefficient (Allocca et al., 2014). A soil cover exerts a fundamental influence on groundwater recharge processes by enhancing water losses to evapotranspiration. The studied case therefore pertains to recharge characteristics of a soil mantled karst aquifer as is very common in southern Italy as well as other areas of the world.

In the period that we analyzed, calendar year 2008, the total amount of precipitation (1779.8 mm) was very close to the mean annual average value of 1730 mm for the Terminio karst aquifer. The portion of precipitation that does not become recharge is lost primarily to evapotranspiration, runoff being considered negligible in this area of endorheic morphology. This negligibility allows considering the annual water losses to evapotranspiration, expressed as a fraction of precipitation, to be the complement of the mean RPR (27%). This value is close to that estimated independently by the Thornthwaite-Mather (1955, 1957) method (about 30%) (Table 3). This close agreement provides a confirmation of both approaches.

Episodes with lower RPR correspond generally to high-intensity rainstorms (e.g. episodes 4 and 11 in Table 2), which may have generated runoff flowing toward the altimetrically lowest sector of the Acqua della Madonna test area. The effect of antecedent soil–water content on RPR is also evident in some non-recharge periods (Figs. 2a, 4a and 7), when there was significant rainfall but no episodic recharge.

Given this phenomenological framework, we obtained new insights regarding local- and episodic-scale recharge with a multiple linear correlation between RPR, rainfall intensity, and antecedent soil–water content. For a constant rainfall intensity, it is interesting that the range of RPR (26%) over the recorded extremes of θ_{av} ($10.0\% \leqslant \theta_{av} \leqslant 43.0\%$) corresponds to the total available water content ($\Delta\theta_{TAW}$ = 26%). This correspondence is related to the fact that water content at a depth of 0.1 m represents a proxy of soil moisture in the whole evapotranspiration zone. It can be understood as a mutual validation of independent estimations and confirmation of the importance of soil moisture stored in the evapotranspiration zone.

Finally, the results give further insights regarding the value and limitations of the monthly soil water balance and the EMR technique for assessment of groundwater recharge. Taking runoff to be negligible, monthly and annual amounts of groundwater recharge indicate a good match of both approaches.

6. Conclusions

The results of this study represent progress in the application and testing of the Episodic Master Recession (EMR) method. The application to a new hydrogeological framework, a heterogeneous perched karst aquifer of southern Italy, demonstrated the method's value where the stratified subsurface includes sharp hydrogeologic contrasts within the zone of water table fluctuation. This is an important step beyond the few cases previously considered, in which the subsurface was effectively homogeneous over the observed water-table range (Nimmo et al., 2015). The results support the usefulness of the EMR method for quantifying recharge processes at local and episodic scales in Mediterranean karst areas and elsewhere. Further insights were discovered at the episodic time scale concerning the dependence of RPR on basic hydrological parameters that control groundwater recharge. Therefore, the prediction of groundwater recharge from basic hydrological data of precipitation and soil–water content may be a powerful tool for sustainable management of karst systems and protection of groundwater-dependent ecosystems. The current context of climate change and the increasing demand for drinking water in various areas of the world intensifies the need for such tools. These findings can be further developed by empirical or numerical approaches, to advance the assessment of episodic groundwater recharge and provide useful tools to manage artificial groundwater recharge.

Acknowledgements

This work was supported by the personnel short mobility and the doctorate programs of the University of Naples Federico II that funded scientific collaboration with the Unsaturated Zone Interest Group (UZIG) of the US Geological Survey. The authors are grateful to Dr. Erik Smith, USGS, Minnesota, for his useful suggestions.

The authors are grateful to the Editor P.K. Kitanidis, the Associate Editor B. Mahler, and the other two anonymous reviewers for their helpful comments.

The authors gratefully acknowledge the journal ''Groundwater'' published by John Wiley & Sons Ltd. for permitting the reuse of Fig. 3.

References

Allocca, V., Celico, F., Celico, P., De Vita, P., Fabbrocino, S., Mattia, S., Monacelli, G., Musilli, I., Piscopo, V., Scalise, A.R., Summa, G., Tranfaglia, G., 2007a. Illustrative Notes of the Hydrogeological Map of Southern Italy. Istituto Poligrafico e Zecca dello Stato, Rome, pp. 1–211 (ISBN 88-448-0223-6).

Allocca, V., De Vita, P., Fabbrocino, S., Celico, P., 2007b. The karst aquifers of the southern Apennines (Italy): a strategic groundwater resource. Memorie Istituto Italiano di Speleologia 2 (19), 65–72.

Allocca, V., Celico, F., Petrella, E., Marzullo, G., Naclerio, G., 2008. The role of land use and environmental factors on microbial pollution of mountainous limestone aquifers. Environ. Geol. 55, 277–283.

Allocca, V., Manna, F., De Vita, P., 2014. Estimating annual groundwater recharge coefficient for karst aquifers of the southern Apennines (Italy). Hydrol. Earth Syst. Sci. 18, 803–817.

Andreo, B., Vías, J., Durán, J.J., Jiménez, P., López-Geta, J.A., Carrasco, F., 2008. Methodology for groundwater recharge assessment in carbonate aquifers: application to pilot sites in southern Spain. Hydrogeol. J. 16, 911–925.

Boni, C.F., Bono, P., Capelli, G., 1986. Schema Idrogeologico dell'Italia Centrale (scala 1:500.000). Mem. Soc. Geol. It. 35 (2), 991–1012.

Bucci, A., Allocca, V., Naclerio, G., Capobianco, G., Divino, F., Fiorillo, F., Celico, F., 2015a. Winter survival of microbial contaminants in soil: an in situ verification. J. Environ. Sci. 27, 131–138.

Bucci, A., Petrella, E., Naclerio, G., Allocca, V., Celico, F., 2015b. Microorganisms as contaminants and natural tracers: a 10-year research in some carbonate aquifers (southern Italy). Environ. Earth Sci. http://dx.doi.org/10.1007/s12665-015-4043-1.

Celico, P., 1978. Schema idrogeologico dell'Appennino carbonatico centro-meridionale. Memorie e Note Istituto di Geologia Applicata, Napoli 14, 1–97.

Celico, P., 1983. Idrogeologia dei massicci carbonatici, delle piane quaternarie e delle aree vulcaniche dell'Italia centromeridionale (Marche e Lazio meridionale, Abruzzo, Molise e Campania). Quaderni della Cassa per il Mezzogiorno 4 (2), 1–203.

Celico, P., 1988. Falda in rete sospese nel massiccio carbonatico del monte Terminio (Campania) ed implicazioni idrogeologiche. L'Appennino Meridionale 1, 99–112.

Celico, F., Celico, P., De Vita, P., Piscopo, V., 2000. Groundwater flow and protection in the Southern Apennines (Italy). Hydrogeology 4, 39–47.

Celico, F., Naclerio, G., Bucci, A., Nerone, V., Capuano, P., Carcione, M., Allocca, V., Celico, P., 2010. Influence of pyroclastic soil on epikarst formation: a test study in southern Italy. Terra Nova 22, 110–115.

Cello, G., Mazzoli, S., 1998. Apennine tectonics in southern Italy: a review. J. Geodyn. 27, 191–211.

Coes, A., Spruill, T., Thomasson, M., 2007. Multiple-method estimation of recharge rates at diverse locations in the North Carolina Coastal Plain, USA. Hydrogeol. J. 5 (4), 773–788.

D'Argenio, B., Pescatore, T., Scandone, P., 1973. Schema geologico dell'appennino meridionale (Campania, Lucania). Atti del Convegno: Moderne vedute sulla geologia dell'appennino. Accademia Nazionale dei Lincei 183, 49–72.

De Vita, P., Allocca, V., Manna, F., Fabbrocino, S., 2012. Coupled decadal variability of the North Atlantic Oscillation, regional rainfall and karst spring discharges in the Campania region (southern Italy). Hydrol. Earth Syst. Sci. 16, 1389–1399.

De Vita, P., Napolitano, E., Godt, J.W., Baum, R.L., 2013. Deterministic estimation of hydrological thresholds for shallow landslide initiation and slope stability models: case study from the Somma-Vesuvius area of southern Italy. Landslides 10, 713–728.

Delin, G., Healy, R., Lorenz, D., Nimmo, J., 2007. Comparison of local- to regional-scale estimates of ground-water recharge in Minnesota, USA. J. Hydrol. 334 (1–2), 231–249.

Fiorillo, F., Pagnozzi, M., Ventafridda, G., 2014. A model to simulate recharge processes of karst massifs. Hydrol. Process. http://dx.doi.org/10.1002/hyp.10353.

Ford, D., Williams, P., 2007. Karst Hydrogeology and Geomorphology. Wiley J. & Sons, Ltd., pp. 1–576, ISBN 978-0-470-84996-5.

Geiger, R., 1954. Landolt-Börnstein-Zahlenwerte und Funktionen aus Physik, Chemie, Astronomie, Geophysik und Technik, alte Serie. vol. 3. Klassifikation der Klimate nach W. Köppen. Springer, Berlin, pp. 603–607.

Guardiola-Albert, C., Martos-Rosillo, S., Pardo-Igúzquiza, E., Durán Valsero, J.J., Pedrera, A., Jiménez-Gavilán, P., Liñán Baena, C., 2014. Comparison of recharge estimation methods during a wet period in a karst aquifer. Groundwater. http://dx.doi.org/10.1111/gwat.12310.

Hartmann, A., Goldscheider, N., Wagener, T., Lange, J., Weiler, M., 2014a. Karst water resources in a changing world: review of hydrological modeling approaches. Rev. Geophys. 52 (3), 218–242.

Hartmann, A., Gleeson, T., Rosolem, R., Pianosi, F., Wada, Y., Wagener, T., 2014b. A simulation model to assess groundwater recharge over Europe's karst regions. Geosci. Model Dev. Discuss. 7, 7887–7935.

Healy, R.W., 2010. Estimating Groundwater Recharge. Cambridge University Press, p. 256, ISBN 978-0-521-86396-4.

Healy, R.W., Cook, P.G., 2002. Using groundwater levels to estimate recharge. Hydrogeol. J. 10, 91–109.

Heppner, C., Nimmo, J., 2005. A computer program for predicting recharge with a master recession curve. U.S. Geological Survey Scientific Investigations Report 2005-5172, pp. 1–8.

Heppner, C.S., Nimmo, J.R., Folmar, G.J., Gburek, W.J., Risser, D.W., 2007. Multiple-methods investigation of recharge at a humid-region fractured rock site, Pennsylvania, USA. Hydrogeol. J. 15 (5), 915–927.

Keller, J., Bliesner, R.D., 1990. Sprinkle and Trickle Irrigation van Nostrand Reinhold, New York, NY, pp. 1–652.

Lerner, D.N., Issar, A.S., Simmers, I., 1990. Groundwater Recharge, A Guide to Understanding and Estimating Natural Recharge, vol. 8. International Association of Hydrogeologists, Kenilworth.

Lorenz, D.L., Delin, G.N., 2007. A regression model to estimate regional groundwater recharge in Minnesota. Ground Water 45 (2), 196–208.

Manna, F., Allocca, V., De Vita, P., Fusco, F., Napolitano, E., 2013a. Groundwater recharge assessment in karst aquifers of southern Apennines (Italy). Rendiconti Online Società Geologica Italiana 24, 202–204.

Manna, F., Allocca, V., Fusco, F., Napolitano, E., De Vita, P., 2013b. Effect of the North Atlantic Oscillation on groundwater recharge in karst aquifers of the Cilento Geopark (Italy). Rendiconti Online Società Geologica Italiana 28, 106–109.

Meinzer, O.E., 1923. The occurrence of groundwater in the United States with a discussion of principles. U.S. Geol. Surv. Water – Supply Pap. 489, 1–321.

Mirus, B.B., Nimmo, J.R., 2013. Balancing practicality and hydrologic realism: a parsimonious approach for simulating rapid groundwater recharge via unsaturated-zone preferential flow. Water Resour. Res. 49, 1458–1465.

Naclerio, G., Petrella, E., Nerone, V., Allocca, V., De Vita, P., Celico, F., 2008. Influence of topsoil of pyroclastic origin on microbial contamination of groundwater in fractured carbonate aquifers. Hydrogeol. J. 16, 1057–1064.

Naclerio, G., Nerone, V., Bucci, A., Allocca, V., Celico, F., 2009. Role of organic matter and clay fraction on migration of Escherichia coli cells through pyroclastic soils, southern Italy. Colloids Surf., B 72, 57–61.

Nimmo, J.R., 2012. Preferential flow occurs in unsaturated conditions. Hydrol. Process. 26 (5), 786–789.

Nimmo, J.R., Horowitz, C., Mitchell, L., 2015. Discrete-storm water-table fluctuation method to estimate episodic recharge. Groundwater 53, 282–292.

Petrella, E., Capuano, P., Celico, F., 2007. Unusual behaviour of epikarst in the Acqua dei Faggi carbonate aquifer (Southern Italy). Terra Nova 19, 82–88.

Petrella, E., Capuano, P., Carcione, M., Celico, F., 2009. A high-altitude temporary spring in a compartmentalized carbonate aquifer: the role of low-permeability faults and karst conduits. Hydrol. Process. 23, 3354–3364.

Petrella, E., Aquino, D., Fiorillo, F., Celico, F., 2014. The effect of low-permeability fault zones on groundwater flow in a compartmentalized system. Experimental evidence from a carbonate aquifer (Southern Italy). Hydrol. Process. http://dx.doi.org/10.1002/hyp.10294, Published online.

Risser, D., Gburek, W., Folmar, G., 2005. Comparison of methods for estimating ground-water recharge and base flow at a small watershed underlain by fractured bedrock in the eastern United States. U.S. Geological Survey Scientific Investigations Report, 2005-5038, p. 31.

Rutledge, A.T., 1998. Computer programs for describing the recession of ground-water discharge and for estimating mean ground-water recharge and discharge from streamflow data-update. Water-Resources Investigations Report 98-4148, US Geological Survey.

Scanlon, B.R., Keese, K.E., Flint, A.L., Flint, L.E., Gaye, C.B., Edmunds, W.M., Simmers, I., 2006. Global synthesis of groundwater recharge in semiarid and arid regions. Hydrol. Process. 20, 3335–3370.

Stephens, D.B., 1995. Vadose Zone Hydrology. CRC Press, p. 339, ISBN-10:0873714326.

Thornthwaite, C.W., 1948. An approach toward a rational classification of climate. Geogr. Rev. 38, 55–94.

Thornthwaite, C.W., Mather, J.R., 1955. The water balance. Publ. Climatol. 8 (1), 1–104.
Thornthwaite, C.W., Mather, J.R., 1957. Instructions and tables for computing potential evapotranspiration and the water balance. Publ. Climatol. 10 (3), 1–311.
Todd, D.K., 1980. Groundwater Hydrology, Third ed. Wiley J., New York, pp. 1–665535, ISBN 0-471-87616-X, 20051980.
VV.AA., 2007. Regional climate projections. Climate change. Cap. 11 in "Climate Change 2007: The Physical Science Basis". In: Solomon, S., Qin, D., Manning, M., Chen, Z., Marquis, M., Averyt, K.B., Tignor, M., Miller, H.L. (Eds.), Contribution of Working Group I to the Fourth Assessment Report of the Intergovernmental Panel on Climate Change. Cambridge University Press, Cambridge, United Kingdom and New York, NY, USA, 996 pp.
Wada, Y., van Beek, L.P.H., van Kempen, C.M., Reckman, J.W.T.M., Vasak, S., Bierkens, M.F.P., 2010. Global depletion of groundwater resources. Geophys. Res. Lett. 37 (1–5), L20402.